

# Numerical and experimental study on flexural behavior of reinforced concrete beams: Digital image correlation approach

B. Murali Krishna\*, V. Guru Prathap Reddy, T. Tadepalli<sup>a</sup>, P. Rathish Kumar and Yerra Lahir

Department of Civil Engineering, National Institute of Technology Warangal, Telangana, 506004, India

(Received July 23, 2019, Revised October 28, 2019, Accepted December 3, 2019)

**Abstract.** Understanding the realistic behavior of concrete up to failure under different loading conditions within the framework of damage mechanics and plasticity would lead to an enhanced design of concrete structures. In the present investigation, QR (Quick Response) code based random speckle pattern is used as a non-contact sensor, which is an innovative approach in the field of digital image correlation (DIC). A four-point bending test was performed on RC beams of size 1800 mm x 150 mm x 200 mm. Image processing was done using an open source Ncorr algorithm for the results obtained using random speckle pattern and QR code based random speckle pattern. Load-deflection curves of RC beams were plotted for the results obtained using both contact and non-contact (DIC) sensors, and further, Moment (M)-Curvature ( $\kappa$ ) relationship of RC beams was developed. The loading curves obtained were used as an input data for material model parameters in finite element analysis. In finite element method (FEM) based software, concrete damage plasticity (CDP) constitutive model is used to predict the realistic nonlinear quasi-static flexural behavior of RC beams for monotonic loading condition. The results obtained using QR code based DIC are observed to be on par with conventional results and FEM results.

**Keywords:** Concrete Damage Plasticity (CDP); DIC; FEM; Moment-Curvature; QR code

## 1. Introduction

A simple, cost effective and practical imaging based technique is proposed for monitoring damage in bridges, dams, buildings, nuclear industry, defence and aerospace structures. DIC is a full-field contactless metrology technique used for condition assessment of civil infrastructure (Mudassar *et al.* 2016). DIC is now extensively used as a practical and effective tool in the field of experimental mechanics for quantitative in-plane deformation measurement of a planar object surface (Sutton *et al.* 2009, Felekoglu and Keskinates 2016). It directly provides full-field displacements to sub-pixel level precision and full-field strains by comparing digital images of a planar test object surface acquired before and after deformation. Comparisons can be made between measured data by capturing precisely positioned with aligned speckle patterns where differences can be readily identified between the surface changes and deformations (Sutton *et al.* 2009, Aggelis *et al.* 2016, Kumar *et al.* 2019).

DIC is used for long term monitoring by imaging structural components periodically, at different locations and further, computing strains and displacements from images recorded at regular intervals of time during operating conditions. DIC is a virtual optical method used to correlate the sequence of images to determine the

similarity among them (Antos *et al.* 2017, Pagani *et al.* 2019). DIC data can be used to track the deterioration history of a defective component. Structural monitoring of individual components (local analysis) of a structure and entire structure (global analysis) can also be studied using DIC. The basic principle of DIC is to determine the surface displacement of a planar test object (Antos *et al.* 2017).

Contact sensor devices are used to measure object distortion while loading the test. The most extensively adopted instruments are linear variable differential transformers (LVDTs), dial gauges and strain gauges, which measure displacement with respect to the rate of loading applied on specimen (Carter *et al.* 2015). These devices are well established, with an accuracy of  $\pm 1\mu\text{m}$  or maybe even lower, where actual real-time data can be captured. On the other hand, these contact sensors can measure in one dimension only, limited to the area where the sensor is fixed. Sensors when used with a controller unit are prone to damage during destructive tests (Yuan *et al.* 2015). Therefore, LVDTs or strain gauges are not suitable in case of extreme testing conditions. Contact sensors are used traditionally for measurement of deformations, but due to inherent difficulties in terms of accuracy, necessity of flat surfaces and issues related to the attachment of these devices, non-contact methods of measurements are becoming popular.

The displacement component on the surface of an object is obtained by recording and correlating the surface images before and after deformation. Speckle patterns are usually created on specimen surfaces for more precise measurement using DIC (Kozicki and Teichman 2007). The size and shape of speckle-pattern generally affect the displacement measurements. Ideal speckle size should be around 3 to 5

\*Corresponding author, Ph.D.

E-mail: [bmurali@student.nitw.ac.in](mailto:bmurali@student.nitw.ac.in)

<sup>a</sup>Assistant Professor

E-mail: [tezeswi@nitw.ac.in](mailto:tezeswi@nitw.ac.in)

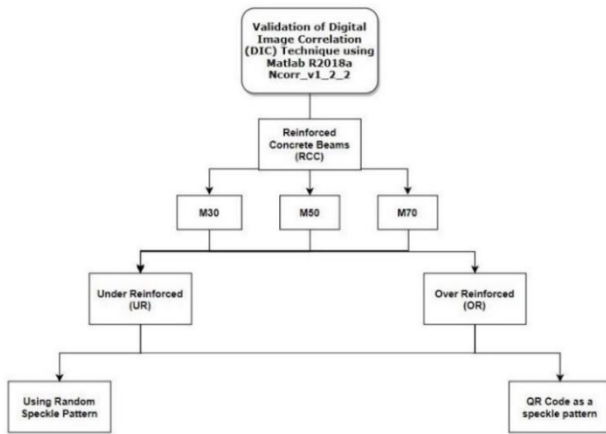


Fig. 1 Schematic view of the experimental program

pixels in order to optimize spatial resolution (Lecompte *et al.* 2006). Generally, the speckle pattern is random and it is hard to achieve a pattern regular enough to cause false matching. The pattern must be either bright white dots on a dark black background or dark black dots on a bright white background (Long *et al.* 2013). To attain effective correlation between the images, the pattern should be isotropic, non-repetitive and have high contrast (Gencturk *et al.* 2014). In order to assist a non-contact strain measurement system, an open source Matlab® based algorithm Ncorr v1.2.2 (Blaber *et al.* 2015) was used as a tool for visualization of loading history from initial unloading stage to failure. This method is relatively easy to set up and deploys a cost-effective ordinary optical digital camera like a digital single-lens reflex camera (DSLR) or smartphone camera, adapted according to the situation (Pan *et al.* 2009, Salmanpour and Mojsilovic 2013, Felekoglu and Keskinates 2016, Suryanto *et al.* 2017).

Several successful implementations of the DIC measurement technique using low cost DSLR cameras have been reported in literature (Salmanpour and Mojsilovic 2013, Dutton *et al.* 2013, Fayyad and Lees 2014). The results proved that DIC is an effective technique to measure full-field displacements and strains with good accuracy and spatial resolution. Furthermore, using low-cost conventional DSLR cameras (compared to special industrial cameras) makes this technique affordable.

This paper presents the experimental and numerical validation of RC beam specimen using DIC method. The main idea is to develop an alternative to traditionally used random speckle pattern in DIC, an innovative new approach to collect data for this traditional 4 point bending experiment using QR code speckle pattern.

## 2. Experimental programme

The experimental design comprises casting 24 beams including three concrete grades M30, M50 and M70 (M means Mix and 30, 50 and 70 implies the characteristic compressive of concrete in Mpa). For each grade, two different types of speckle-pattern are used, with under-reinforced (UR) and over-reinforced (OR) sections. The



(a) Random speckle pattern



(b) QR code based random speckle pattern

Fig. 2 Testing of beams using DIC Speckle Pattern

details of the specimens tested are shown in Fig. 1.

### 2.1 Specimen preparation and testing

The reinforced concrete beams of three different grades of concrete M30, M50 and M70 for both UR and OR sections are cast and tested for deformations using dial gauges and curvature meters simultaneously DIC technique was used to obtain the deformations. The unsupported length of RC beams is 1800 mm with a cross section size of 150 mm width and 200 mm depth. The aim of the study is to check the suitability of employing both random speckle pattern and QR based random speckle pattern for the beams. The details of testing of RC beam in progress are shown in Fig. 2.

Dial gauges and curvature meters are used as contact sensors placed at the bottom surface of the RC beam to find out the deflections and rotations. The least count of dial gauges used for deflection measurement was 0.01 mm. The positions of dial gauges and curvature meters are shown in Fig. 3. Curvature meters are used in tension and compression zones and are 200 mm apart from the middle frames. The curvature is measured by placing curvature meters at the top (compression) and bottom (tension) fibers of tested beams. Least count of curvature meters is 0.001 mm which is fixed at the top and bottom of the rectangular frames. The schematic drawing of the equipment used for testing RC beams using a QR code based random speckle pattern painted throughout the cross-section is shown in Fig. 3.

The beams are quasi-statically tested under 1000 KN capacity Universal Testing Machine (UTM) with a displacement rate of 1.5 mm/min. As soon as testing starts, images of the RC beam are taken continuously with the help of Nikon D5200 with a lens of  $f=55$  mm (DSLR camera), without interrupting the testing process. The specifications

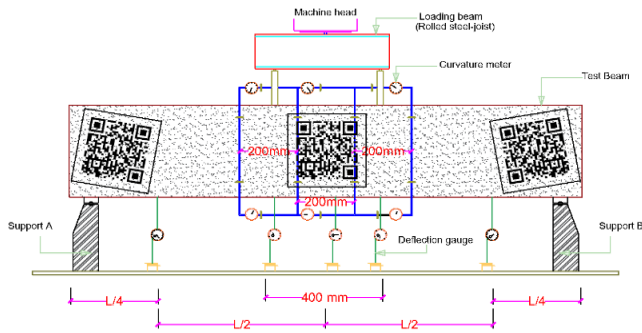


Fig. 3 Schematic representation of RC beam using QR code based random speckle

Table 1 Camera parameters

Width	6000 pixels
Height	4000 pixels
Horizontal resolution	300 dpi
Vertical resolution	300 dpi
Pixel depth	24 bit
Manufacturer	NIKON CORPORATION
Model	Nikon DSLR Camera D5200
Colour display	sRGB
Shutter speed	1/125 S
Aperture	f/3.5
Iris Aperture	w/o flash
Focal length	18mm
Focal ratio	f/3.5
Exposure time	1/125 S
ISO speed	ISO-400
Exposure compensation	0

of the camera used are shown in Table 1. The camera is set in front of the specimen and consecutive images are captured with respect to rate of loading (consecutive intervals). These static images are used for DIC technique using image processing Ncorr v1.2.2 Matlab® R2018a programming software. Using greyscale images, DIC analysis was done and then compared with conventional results obtained from dial gauges and curvature meters.

### 3. Two Dimensional (2D) DIC system

#### 3.1 General principle

DIC works on the basis of comparing digital images of a test component at regular intervals of deformation. The DIC system measures surface deformations, builds full-field 2D vector fields and strain maps by tracing subsets of pixels. DIC technique works effectively when the pixel subsets are random and unique with a range of contrast and intensity levels. The natural surface of the structure/component does not need any special surface preparation for working with DIC, since it has already acquired sufficient image texture. DIC can be used to measure the surface deformation up to one part per million of the field-of-view. Images can be obtained from a variety of sources such as consumer digital

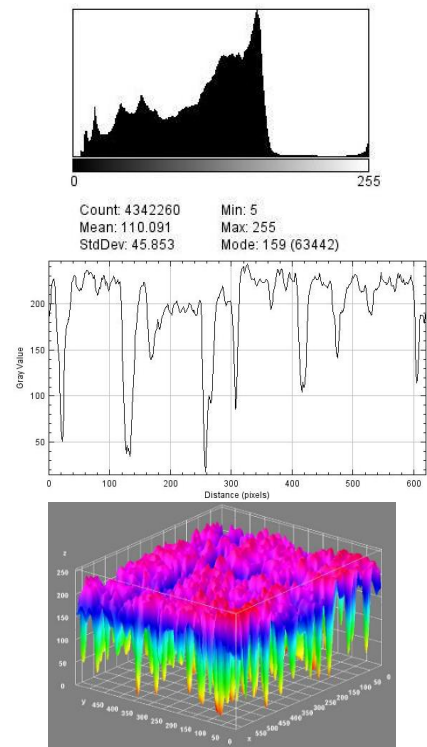


Fig. 4 Surface histogram of RC beam showing grey scale intensity for random speckle pattern

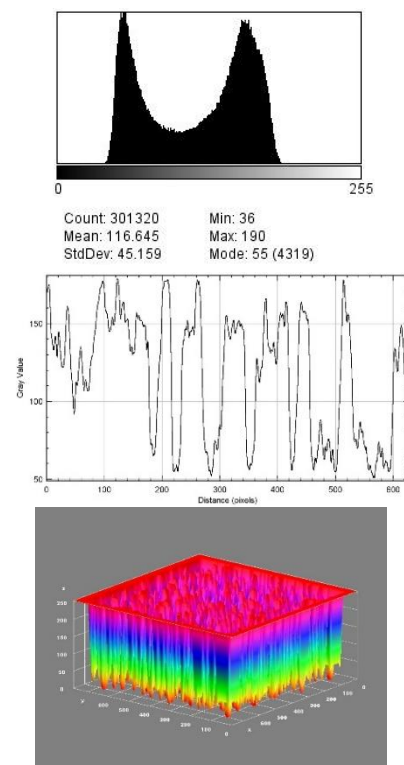


Fig. 5 Surface histogram of RC beam showing grey scale intensity for QR code based random speckle pattern

cameras and conventional Charge Coupled Device (CCD), etc. To work effectively, pixel displacement is converted into engineering units using Ncorr V1.2.2 algorithm. The pixel subsets must be unique and random with a range of

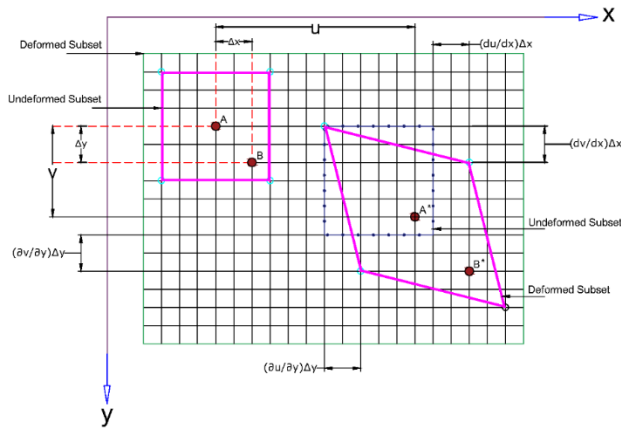


Fig. 6 Schematic representation of subsets before and after deformation

contrast of 8-bit grey scale image intensity levels varying from 1 to 255 as shown in Figs. 4 and 5.

The captured images are pre-processed from RGB colour to grey scale (8-bit) and then analyzed using ImageJ software. Greyscale images have distinct black and white colours. The greyscale value varies from 0 to 256 (0 indicates black; 256 indicates white and the values in between represents different shades of grey). The grey image value of pixel is stored based on the intensity of light. Histogram is a graphical representation of a number of pixels with different intensity values of the image. Histogram can identify pixel values at each point in an image and show the total number of pixels in an image.

### 3.2 DIC terminology

Digital images are divided into a number of smaller regions, which are termed as subsets, and these subsets undergo deformations when the image distortion takes place

shown in Fig. 6. The deformation location of the subset might not be at the integer location. That is why interpolation functions are needed to be used to get the grey intensity value at a non-integer location.

The correlation function (C) is defined as the similarities between the subsets of the image in un-deformed state and in deformed state (Eq. (1)). In general, the Pearson correlation coefficient lies between (-1 to +1) for optimal speckle patterns. To correlate the similarity index between the reference image subset and deformed image subset, a correlation analysis is done as shown in Fig. 7. In order to obtain the deformation subset, 2D DIC algorithm arrives at values of the extreme correlation cost function. This function can be written as

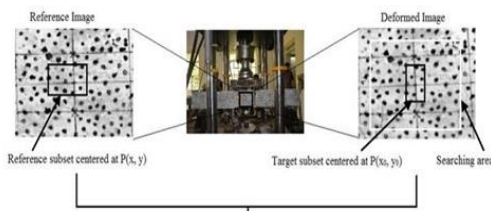
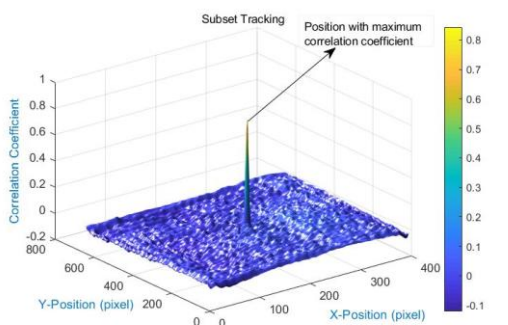
$$C = \frac{\int_{\Delta M} (F(x,y)) (G(x_0+U,y_0+V)) dA}{[\int_{\Delta M} [F(x,y)]^2 dA \int_{\Delta M} [G(x_0+U,y_0+V)]^2 dA]^{1/2}} \quad (1)$$

Where,  $F$  and  $G$  are greyscale intensity functions at a specified location  $(x, y)$  and  $(x_0, y_0)$  of reference images and deformed images respectively.

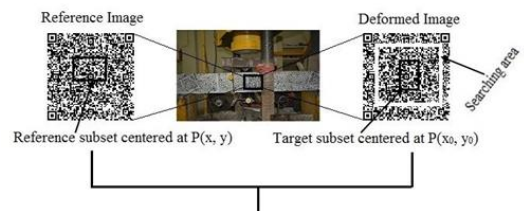
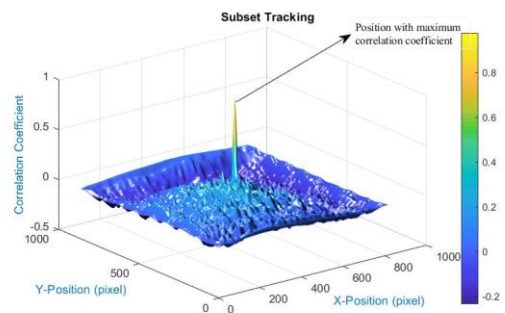
The physical size of pixel depends upon the field of view (FOV). The intention behind using the DIC technique widely is due to the drop down prices of CCD and Complementary Metal-Oxide-Semiconductor (CMOS) sensor based cameras. DIC compares optical photographs of the test piece/component at different stages of deformation by identifying the subsets of pixels as shown in Fig. 8. The system can also measure surface deformation and come up with full field 2D deformation vector fields and strain maps.

### 3.3 Computation of strain measurement

The measured displacement fields  $(u, v, w)$  are converted into Cartesian coordinate system  $(x, y, z)$  and the strain metrics are calculated as shown in Eqs. (2)-(4). Displacement gradients are determined in order to get the strain at any point in a body. The four displacement



(a) Using random speckle pattern



(b) Using QR code random speckle pattern

Fig. 7 Subset tracking procedure using DIC

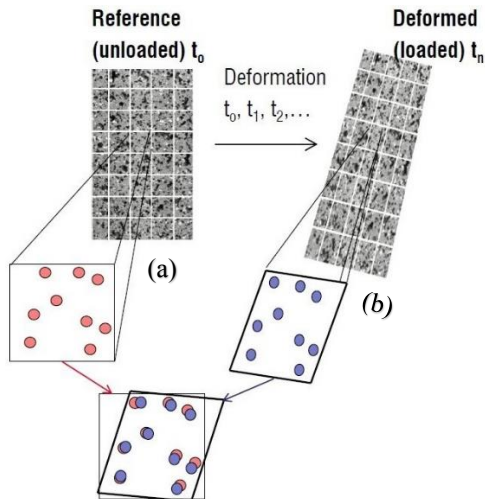


Fig. 8 Pictorial representation of subsets (a) Reference subset before deformation, (b) Target subset after deformation



Fig. 9 QR code Stencil pattern

gradients are used to find the Lagrangian strains, which are as follows

$$E_{xx} = 0.5 \left[ 2 \frac{\partial u}{\partial x} + \left( \frac{\partial u}{\partial x} \right)^2 + \left( \frac{\partial v}{\partial x} \right)^2 \right] \quad (2)$$

$$E_{xy} = 0.5 \left[ \frac{\partial u}{\partial y} + \frac{\partial v}{\partial x} + \frac{\partial u}{\partial x} \frac{\partial u}{\partial y} + \frac{\partial v}{\partial x} \frac{\partial v}{\partial y} \right] \quad (3)$$

$$E_{yy} = 0.5 \left[ 2 \frac{\partial v}{\partial y} + \left( \frac{\partial u}{\partial y} \right)^2 + \left( \frac{\partial v}{\partial y} \right)^2 \right] \quad (4)$$

### 3.4 QR code based DIC technique

DIC technique has been utilized successfully for large deformation measurements. Due to its simplicity, the DIC technique has been further extended to curvature studies. According to the technique, if the specimen attains the natural texture of random grey intensity value, there is no need to prepare the surface of the specimen. The size of the QR code sprayed on the beam is 150 mm by 150 mm, as shown in Fig. 9. The minimum radius of the subset considered in this study was 1.5 mm escribed circle, with a step size of 1.5 mm up to 21 mm, because there was no significant difference in the results after 18 mm until 21 mm. The ideal radius of subset was found to be 13 mm based on the results obtained, which are on par with

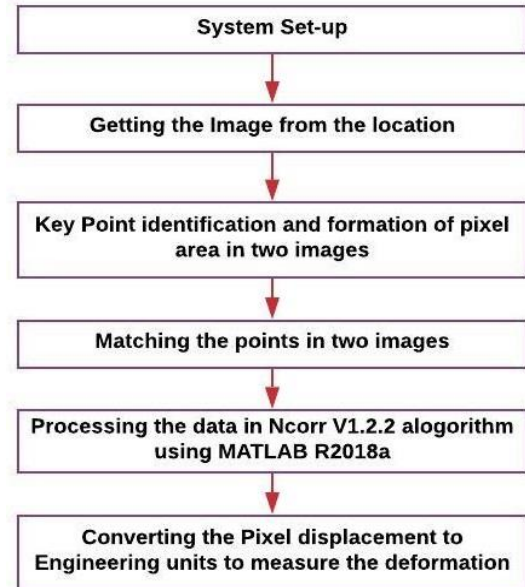


Fig. 10 Flowchart showing the image processing technique

conventional results. Flowchart showing the image processing technique in Fig. 10, explains the procedure adopted for DIC technique.

QR code based speckle pattern finds applications in real-time field structural health monitoring (Meadati *et al.* 2015). As QR code is being used for numerous applications in data encryption, data transmission and as information carrier in web applications. Therefore, using QR code as a speckle pattern for DIC in real-time structural health monitoring provides us with certain advantages such as the QR code being encrypted with details of the structure helps in easy identification of the structure by scanning.

The aim of this study is to use QR code based speckle pattern, verify and validate its results with currently used random speckle pattern in DIC. From this study, it was observed that QR code based speckle pattern is on par with or slightly better than random speckle pattern (refer section 5).

## 4. Finite Element Method

Finite Element Method (FEM) is a numerical simulation method to obtain solutions to problems, which otherwise are difficult to obtain. In FEM, the solution to a problem is obtained by dividing a larger system into several smaller parts, which are called finite elements (discretization) (Grassl *et al.* 2013, Kalyana Rama *et al.* 2017). In this paper concrete damage plasticity (CDP) constitutive model is used for modelling concrete, available in standard numerical tool ABAQUS v6.14/CAE (FEM software), which is a powerful engineering numerical simulation program. With the help of this tool, the results obtained from experimental tests on RC beams for different grades of concrete are validated. A normal plasticity model is used to simulate the nonlinear monotonic behavior of steel in concrete. The numerical results are in line with the conventional results obtained from contact and contactless

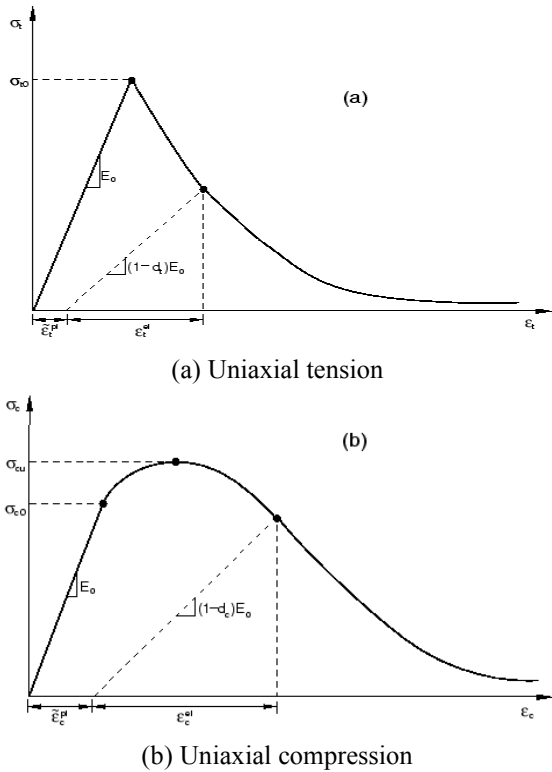


Fig. 11 The stress-strain behavior of concrete (ABAQUS6 2011)

measurement techniques. The flexural response of RC beams obtained using DIC is compared with those obtained from conventional tests and numerical simulations.

4.1 Concrete Damage Plasticity (CDP) model

Concrete structures necessitate the use of advanced numerical analysis, which requires using nonlinear discretization of material model with finite element simulation. The beam is modeled using CDP constitutive model, available in ABAQUS v6.14/CAE software, which is suitable for modeling both plain and reinforced concrete, under varying types of static and dynamic loads such as monotonic, cyclic etc. The concrete behavior in the axial concrete damaged plasticity model was given by Lubliner *et al.* (1989) and the yield surface of this model was later modified by Lee and Gregory (1998). In this model, it is assumed that the concrete fails mainly due to tensile cracking and crushing of concrete due to compression. The combined behavior of steel and concrete is replicated by using “embedded element technique”. CDP model assumes non-associated plastic flow. The flow potential  $G$  used in the present investigation is based on Drucker-Prager hyperbolic function as shown in Eq. (5).

$$G = \sqrt{(\epsilon \sigma_{t0} \tan \Psi)^2 + \bar{q}^2} - \bar{p} \tan \Psi \tag{5}$$

Where,

- $\sigma_{t0}$  - Uniaxial tensile stress at failure
- $\bar{p}$  - Hydrostatic pressure stress
- $\bar{q}$  - Mises equivalent effective stress
- $\Psi$  - Dilation angle

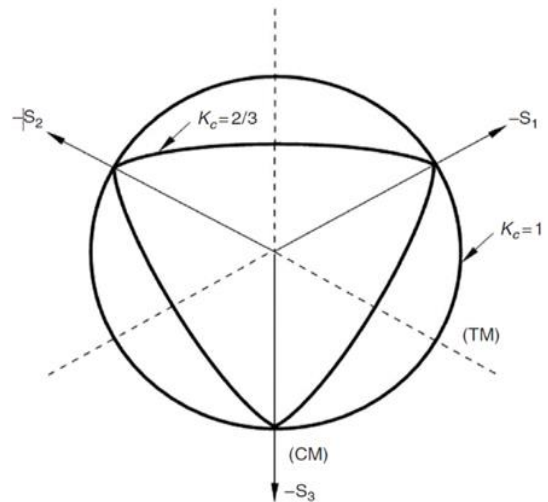


Fig. 12 CDP deviatoric plane for different values of KC (Jankowiak and Lodygowski 2005)

Table 2 Input parameters used in CDP

$\Psi$	dilation angle	35°
$e$	eccentricity	0.1
$F$	$\sigma_{bo}/\sigma_{co}$	1.12
$K_c$	$q_{TM}/q_{CM}$	0.67
Viscosity parameter		0

Table 3 Input parameters used in CDP

Concrete compression damage		Concrete tension damage	
Damage parameter C	Inelastic strain	Damage parameter T	Cracking strain
0	0.000828016	0	0
0.81	0.003573541	0.99	0.001494322

$\epsilon$  - Eccentricity

The accurate material modeling is the most challenging aspect in finite element modeling of concrete structures and especially the modeling of concrete. The stress-strain behavior of concrete (i.e., uniaxial tensile and compressive response of concrete) is characterized by damaged plasticity, as shown in Fig. 11.

The strength of concrete under uniaxial tension and compression was used to identify the shape of flow potential and the corresponding load surfaces. The changes made for the CDP model was that the failure surface considered in the deviatoric plane need not be a circle as shown in Fig. 12, and the shape of deviatoric plane is given by a parameter  $K_c$ . As recommended by the user’s manual of ABAQUS, the failure surface for  $K_c=2/3$  was used in the analysis.

The input parameters used in the analysis by CDP constitute models which are shown in Tables 2-3 taken from ABAQUS User’s manual (2013).

4.2 Simulation modeling

Non-linear 3D solid finite element numerical analysis was performed on RC beam under four-point loading test to

Table 4 Reinforcement details of RC tested beams

Beam Designation	Top bars (mm)	Bottom bars (mm)	8 $\phi$ stirrups spacing (mm)
M30 UR	2-8 $\phi$	3-10 $\phi$	130
M30 OR	2-8 $\phi$	2-16 $\phi$ , 2-10 $\phi$	95
M50 UR	2-8 $\phi$	4-12 $\phi$	75
M50 OR	2-8 $\phi$	3-20 $\phi$	60
M70 UR	2-8 $\phi$	3-16 $\phi$	75
M70 OR	2-8 $\phi$	4-20 $\phi$	50

Table 5 Concrete and reinforcement steel properties used in simulation model

Grade of Concrete (MPa)	Concrete Mechanical Properties			Steel Properties	
	Density (kg/m <sup>3</sup> )	Elastic Modulus (MPa)	Poisson's ratio	Density (kg/m <sup>3</sup> )	Poisson's ratio
M30	2400	27400	0.15	7850	0.3
M50	2400	35350	0.15	7850	0.3
M70	2400	41830	0.15	7850	0.3

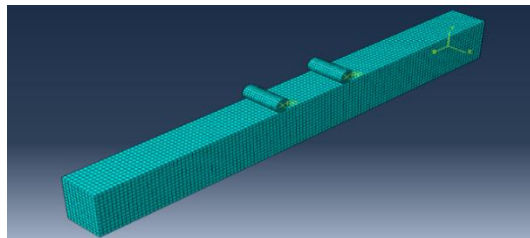


Fig. 13 Meshed RC beam

determine its ultimate moment capacity. The geometry of rebar sections and concrete beam sections were created in ABAQUS. These sections can be extruded in 3D space. A solid 3D deformable model of the Reinforced Concrete Beam with 200 mm depth and 150 mm width with a length of 1800 mm was developed. Reinforcement of length 1800 mm and appropriate stirrups (dimensions are given in Table 4) for M30, M50, M70 (OR and UR) beams were developed. Properties of both concrete and rebar materials used in simulations were created in property module and assigned to the respective parts and are shown in Table 4 and Table 5.

In numerical simulation, concrete specimen was loaded by creating a rigid body surface (applicator) and imparting load to the applicator. Between rigid body surface and concrete beam specimen, where the load is applied, contact conditions were used. Hence, the pressure force applied on the specimen was distributed to replicate experimental conditions. Using an embedded region option in ABAQUS constraints tab, rebars were embedded in concrete with the same degrees of freedom, hence, creating a perfect bond between concrete and rebar. For meshing concrete, an 8-noded linear brick element (C3D8R element) with reduced integration formulation was used. For meshing rebar, T3D2 (Truss element) a 2-noded linear 3D truss element was used in modeling. The geometry of the meshed RC beam is shown in Fig. 13.

Pinned support boundary condition was given on both the sides of RC beam at 100 mm from the edges (in initial

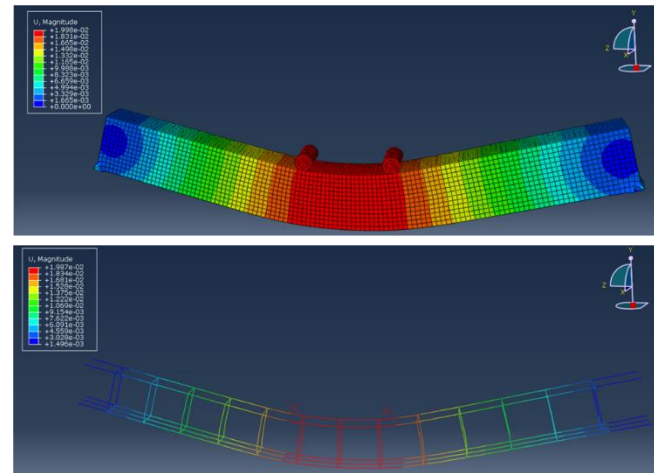
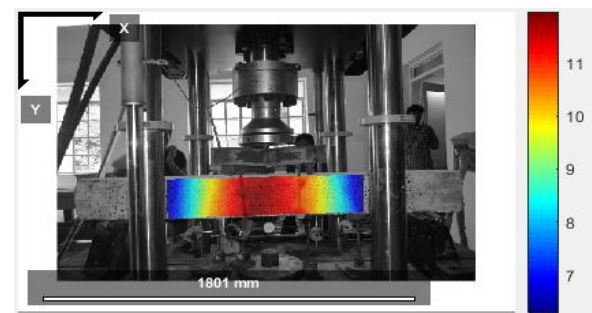
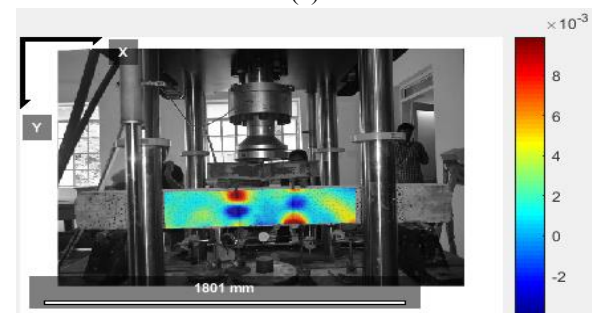


Fig. 14 Deflection profile of RC beam



(a)



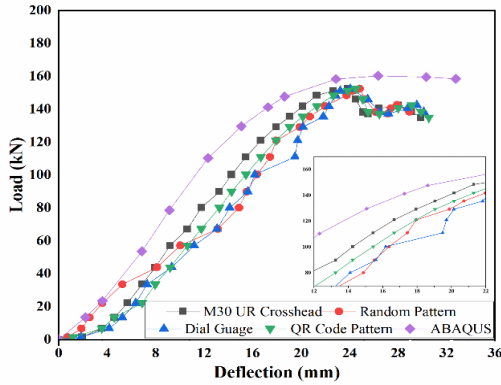
(b)

Fig. 15 Deflection profile using Ncorr V1.2.2 (a) Vertical Displacement (mm), (b) Horizontal Displacement (mm)

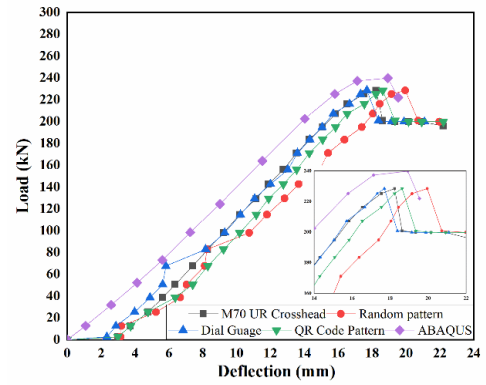
step). Also, applicator was given a boundary condition to move only in the direction of loading. Step1 was created and load was assigned using displacement control. The deflections at the end of analysis for the entire beam and reinforcements within is shown in Fig. 14. Comparison of simulation results with both DIC and conventional mid-span deflection was done.

## 5. Results and discussions

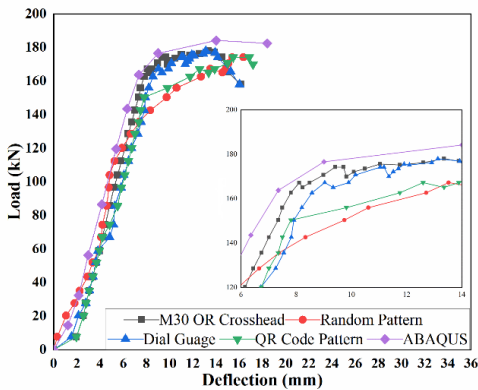
DIC results are compared with standard numerical tool ABAQUS v6.14/CAE software and conventional results obtained using dial gauges and actuator data for both the specimens. A 3D solid finite element analysis ABAQUS® 6.14/CAE numerical simulation tool is used to validate the



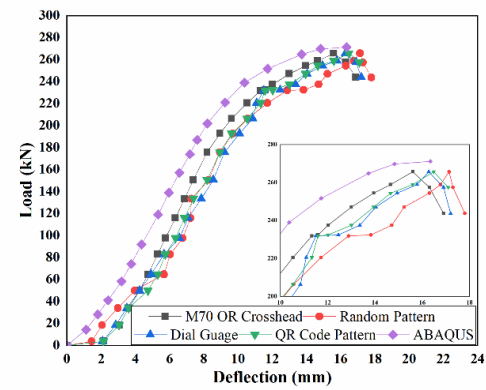
(a) M30 UR RC beam



(a) M70 UR RC beam



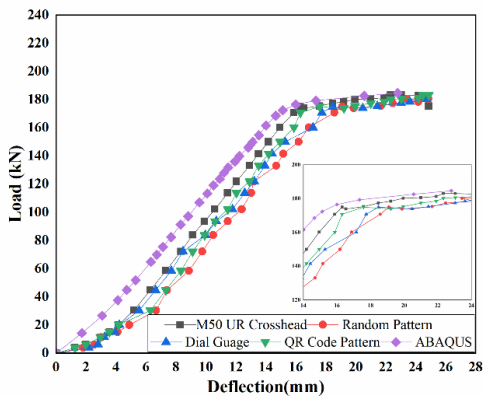
(b) M30 OR RC beam



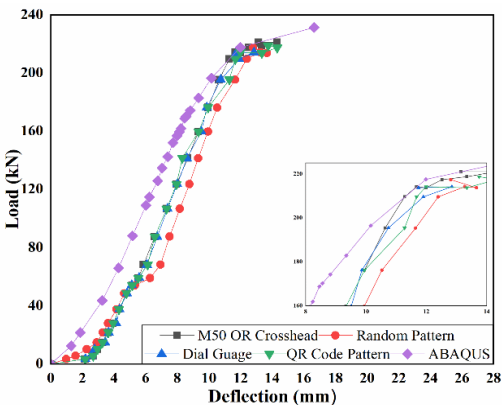
(b) M70 OR RC beam

Fig. 16 Load vs deflection plots

Fig. 18 Load vs Deflection plots



(a) M50 UR RC beam



(b) M50 OR RC beam

Fig. 17 Load vs deflection plots

results obtained from RC beams of both conventional and DIC measurements.

### 5.1 Load-deflection curves

The deflection curves are plotted with the corresponding loads obtained from the UTM using the results obtained from both conventional and DIC analysis. These curves are also compared with FEM results. The deflection profile of random pattern obtained using DIC software is shown in Fig. 15. The load-deflection curves are plotted using DIC and compared with conventional crosshead motion of RC beam and FEM results shown in Figs. 16-18. The average load-deflection curves plotted are taken as the average of two beams.

### 5.2 Moment-Curvature ( $M-\kappa$ ) relationship

$M-\kappa$  relationship developed with the results obtained using DIC is compared with results developed using conventionally obtained results and FEM results. The method adopted for developing  $M-\kappa$  relationship is similar (MLV Prasad and Rathish 2012, Dutton *et al.* 2013, Swamy Naga Ratna Giri *et al.* 2018). It is observed that the moment carrying capacity of UR beams is less than OR beams. The grade of concrete increases with the moment carrying capacity, while the curvature of the beam at ultimate moment will decrease as shown in Figs. 19-21. It is observed that the conventional and numerical results are

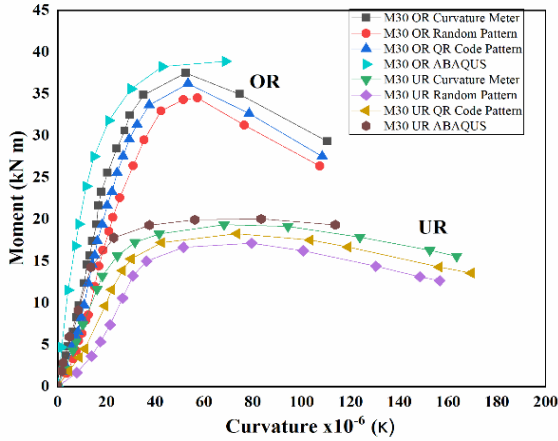


Fig. 19  $M-\kappa$  curve for M30 grade of concrete

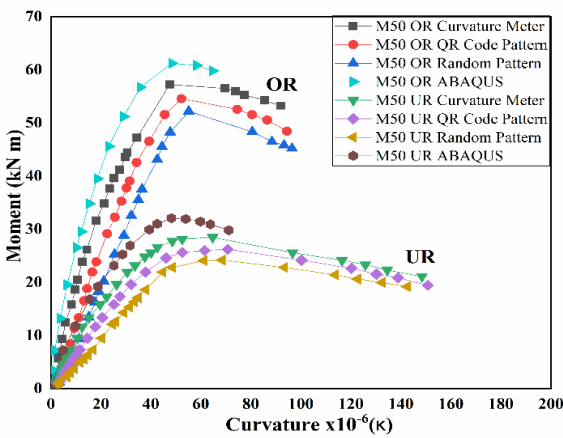


Fig. 20  $M-\kappa$  curve for M50 grade of concrete

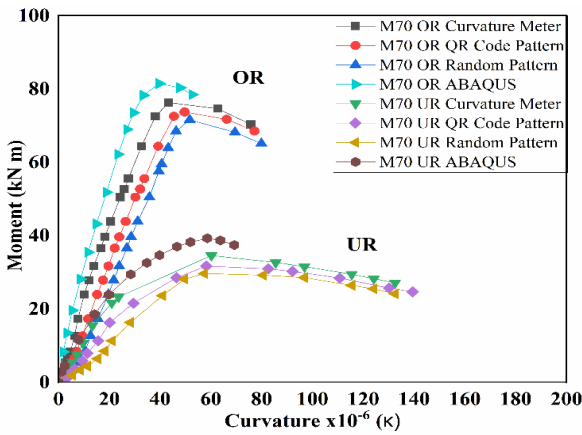


Fig. 21  $M-\kappa$  curve for M70 grade of concrete

in close correlation with those of DIC technique.

From Table 6, it can be observed that, higher moment capacities for RC beams were consistently observed in case of QR code based random speckle pattern when compared to random speckle pattern. From Table 7, it can be observed that the mean absolute error percentage in the ultimate moment is 7.85% in case of FEM results and it reduces to 5.56% for the results obtained from DIC using QR code based random speckle pattern. The mean absolute error percentage in ultimate curvature is 10.75% in case of FEM

Table 6 Comparison of ultimate  $M-\kappa$  results obtained from contact and non-contact sensors

Specimens Designation	Conventional		Random speckle pattern		QR code speckle pattern					
	$M$	$\kappa$	$M^1$	$\kappa^1$	$M$	$\kappa$	$M^1$	$\kappa^1$		
M30 UR	19.36	68.24	17.13	79.49	11.51	16.48	18.27	73.46	5.63	7.64
M30 OR	37.52	52.51	34.52	57.34	7.99	9.19	36.22	53.47	3.46	1.82
M50 UR	28.51	64.78	24.24	68.56	14.97	5.83	26.24	70.77	7.96	9.24
M50 OR	57.25	47.53	52.22	55.19	8.78	16.11	54.59	52.27	4.64	9.97
M70 UR	34.53	60.22	29.65	57.53	14.13	4.44	31.66	58.25	8.31	3.27
M70 OR	76.29	43.36	71.56	51.66	6.20	19.14	73.72	49.69	3.36	14.59
MAE					10.59	11.86	5.56		7.75	

MAE: Mean Absolute Error;  $M^1$ : % error in moment (kN-m);  $\kappa^1$ : % error in curvature

Table 7 Comparison of ultimate  $M-\kappa$  results obtained from experimental and numerical

Specimens Designation	Conventional		FEM results			
	$M$	$\kappa$	$M$	$\kappa$	$M^1$	$\kappa^1$
M30 UR	19.36	68.24	20.04	79.26	3.51	16.14
M30 OR	37.52	52.51	38.87	61.72	3.59	17.53
M50 UR	28.51	64.78	32.08	53.25	12.52	17.79
M50 OR	57.25	47.53	61.24	48.42	6.96	1.87
M70 UR	34.53	60.22	39.28	58.64	13.75	2.62
M70 OR	76.29	43.36	81.46	39.65	6.77	8.55
MAE					7.85	10.75

MAE: Mean Absolute Error;  $M^1$ : % error in moment (kN-m);  $\kappa^1$ : % error in curvature

results and it reduces to 7.75% for the results obtained from DIC using QR code based random speckle pattern. The results obtained from DIC using QR code based random speckle pattern are in good agreement with both conventional as well as FEM results.

## 6. Conclusions

The nonlinear flexural behavior of RC beams for both UR (under reinforced) and OR (over reinforced) beams were tested using random speckle pattern as well as QR code based random speckle pattern. Load-Deflection graphs were plotted for both specimens and Moment ( $M$ )–Curvature ( $\kappa$ ) relationship was obtained using RC beams for with M30 (normal), M50 (medium) and M70 (high) compressive strengths. The following conclusions are drawn:

- The nonlinear constitutive modeling adopted here in, is a CDP model applied in the finite element code, ABAQUS. This constitutive model is used to predict the realistic flexural nonlinear behavior of RC beams, and it is observed that  $M-\kappa$  results extracted using QR code based random speckle pattern are on par with FEM simulation results.
- The FEM results confirm the capability of the proposed model for predicting the nonlinear behavior of concrete in RC beams.
- The more random the pattern is the closer are the DIC

results obtained from both FEM and conventional measurements.

- The QR code based random speckle pattern has dual advantage of data encryption and for consistently real time monitoring using non-contact optical sensors.
- The investigation method and analysis of the proposed material model can be used in future parametric studies on different aspects that influence the flexural failure in RC beams.

## Acknowledgments

This study was funded by MHRD-IMPRINT Grant No: 7338. The authors would like to thank the National Institute of Technology, Department of Civil Engineering Warangal for providing research facilities to carry out this research work.

## References

- ABAQUS (2011), Theory Manual, Dassault Systemes Simulia Corp., Providence, RI.
- Aggelis, D.G., Verbruggen, S., Tsangouri, E., Tysmans, T. and Van Hemelrijck, D. (2016), "Monitoring the failure mechanisms of a reinforced concrete beam strengthened by textile reinforced cement using acoustic emission and digital image correlation", *Smart Struct. Syst.*, **17**(1), 91-105. <https://doi.org/10.12989/sss.2016.17.1.091>.
- Antoš, J., Nežerka, V. and Somr, M. (2017), "Assessment of 2d-dic stochastic patterns", *Acta Polytechnica CTU Proc.*, **13**(1-10). <https://doi.org/10.14311/APP.2017.13.0001>.
- Blaber, J., Adair, B. and Antoniou, A. (2015), "Ncorr: open-source 2D digital image correlation matlab software", *Exper. Mech.*, **55**(6), 1105-1122. <https://doi.org/10.1007/s11340-015-0009-1>.
- Carter, J.L., Uchic, M.D. and Mills, M.J. (2015), "Impact of speckle pattern parameters on DIC strain resolution calculated from in-situ SEM experiments", *Fract. Fatig. Fail. Damage Evol.*, **5**, 119-126. [https://doi.org/10.1007/978-3-319-06977-7\\_16](https://doi.org/10.1007/978-3-319-06977-7_16).
- Dutton, M., Take, W.A. and Hout, N.A. (2013), "Curvature monitoring of beams using digital image correlation", *J. Bridge Eng.*, **19**(3), 05013001. [https://doi.org/10.1061/\(ASCE\)BE.1943-5592.0000538](https://doi.org/10.1061/(ASCE)BE.1943-5592.0000538).
- Fayyad, T.M. and Lees, J.M. (2014), "Application of digital image correlation to reinforced concrete fracture", *Procedia Mater. Sci.*, **3**, 1585-1590. <https://doi.org/10.1016/j.mspro.2014.06.256>.
- Felekoglu, B. and Keskinates, M. (2016), "Multiple cracking analysis of HTPP-ECC by digital image correlation method", *Comput. Concrete*, **17**(6), 831-848. <https://doi.org/10.12989/cac.2016.17.6.831>.
- Gencturk, B., Hossain, K., Kapadia, A., Labib, E. and Mo, Y.L. (2014), "Use of digital image correlation technique in full-scale testing of prestressed concrete structures", *Measure.*, **47**, 505-515. <https://doi.org/10.1016/j.measurement.2013.09.018>.
- Grassl, P., Xenos, D., Nyström, U., Rempling, R. and Gylltoft, K. (2013), "A damage-plasticity approach to modelling the failure of concrete", *Int. J. Solid. Struct.*, **50**(24), 3805-3816. <https://doi.org/10.1016/j.ijsolstr.2013.07.008>.
- Jankowiak, T. and Lodygowski, T. (2005), "Identification of parameters of concrete damage plasticity constitutive model", *Found. Civil Environ. Eng.*, **6**(1), 53-69.
- Kalyana Rama, J.S., Chauhan, D.R., Sivakumar, M.V.N., Vasan, A. and Murthy, A.R. (2017), "Fracture properties of concrete using damaged plasticity model-A parametric study", *Struct. Eng. Mech.*, **64**(1), 59-69. <https://doi.org/10.12989/sem.2017.64.1.059>.
- Kozicki, J. and Tejchman, J. (2007), "Experimental investigations of strain localization in concrete using Digital Image Correlation (DIC) technique", *Arch. Hydro-Eng. Environ. Mech.*, **54**(1), 3-24.
- Kumar, A., Vishnuvardhan, S., Murthy, A.R. and Raghava, G. (2019), "Tensile and fracture characterization using a simplified digital image correlation test set-up", *Struct. Eng. Mech.*, **69**(4), 467-477. <https://doi.org/10.12989/sem.2019.69.4.467>.
- Lecompte, D., Sol, H., Vantomme, J. and Habraken, A. (2006), "Analysis of speckle patterns for deformation measurements by digital image correlation", SPECKLE06: Speckles, From Grains to Flowers, *Int. Soc. Opt. Photon.*, **6341**, 63410E.
- Lee, J. and Fenves, G.L. (1998), "Plastic-damage model for cyclic loading of concrete structures", *J. Eng. Mech.*, **124**(8), 892-900. [https://doi.org/10.1061/\(ASCE\)0733-9399\(1998\)124:8\(892\)](https://doi.org/10.1061/(ASCE)0733-9399(1998)124:8(892)).
- Long, X., Fu, S., Qi, Z., Yang, X. and Yu, Q. (2013), "Digital image correlation using stochastic parallel-gradient-descent algorithm", *Exp. Mech.*, **53**(4), 571-578. <https://doi.org/10.1007/s11340-012-9667-4>.
- Lublimer, J., Oliver, J., Oller, S. and Oñate, E. (1989), "A plastic-damage model for concrete", *Int. J. Solid. Struct.*, **25**(3), 299-326. [https://doi.org/10.1016/0020-7683\(89\)90050-4](https://doi.org/10.1016/0020-7683(89)90050-4).
- Meadati, P. and Irizarry, J. (2015), "BIM and QR code for operation and maintenance", *Comput. Civil Eng.*, 556-563. <https://doi.org/10.1061/9780784479247.069>.
- Mudassar, A.A. and Butt, S. (2016), "Improved digital image correlation method", *Opt. Laser. Eng.*, **87**, 156-167. <https://doi.org/10.1016/j.optlaseng.2015.10.002>.
- Pagani, A., Zappino, E., de Miguel, A. G., Martilla, V. and Carrera, E. (2019), "Full field strain measurements of composite wing by digital image correlation", *Adv. Aircraft Spacec. Sci.*, **6**(1), 69-86. <https://doi.org/10.12989/aas.2019.6.1.069>.
- Pan, B., Qian, K., Xie, H. and Asundi, A. (2009), "Two-dimensional digital image correlation for in-plane displacement and strain measurement: a review", *Measur. Sci. Technol.*, **20**(6), 062001.
- Prasad, M.L.V. and Kumar Rathish, P. (2012), "Moment-curvature relationship of glass fiber reinforced self-compacting recycled aggregate concrete", *J. Environ. Res. Develop.*, **7**(2A).
- Salmanpour, A.H. and N. Mojsilovic. (2013), "Application of digital image correlation for strain measurements of large masonry walls", *Conference Proceedings APCOM & ISCM, Singapore*.
- Suryanto, B., Tambusay, A. and Suprobo, P. (2017), "Crack mapping on shear-critical reinforced concrete beams using an open source digital image correlation software", *Civil Eng. Dimens.*, **19**(2), 93-98. <https://doi.org/10.9744/ced.19.2.93-98>.
- Sutton, M.A., Orteu, J.J. and Schreier, H. (2009), *Image Correlation for Shape, Motion and Deformation Measurements: basic Concepts, Theory and Applications*, Springer Science & Business Media.
- Swamy Naga Ratna Giri, P., Rajesh Kumar, G., Sri Rama Chand, M. and Rathish Kumar, P. (2018), "Flexural behaviour of tie-confined self-curing self-compacting concrete", *Mag. Concrete Res.*, **70**(23), 1232-1242. <https://doi.org/10.1680/jmacr.17.00338>.
- Yuan, Y., Huang, J., Fang, J., Yuan, F. and Xiong, C. (2015), "A self-adaptive sampling digital image correlation algorithm for accurate displacement measurement", *Opt. Laser. Eng.*, **65**, 57-63. <https://doi.org/10.1016/j.optlaseng.2014.05.006>.